Ventricular Helix Angle Trends and Long-Range Connectivity

Alexander J. Wilson[⋆,1,2][0000−0002−5438−9707], Q. Joyce Han[⋆,3][0000−0001−7089−1767] ⋆, Luigi E. Perotti[4][0000−0002−9010−2144], and Daniel B. Ennis[1,2][0000−0001−7435−1311]

[1] Department of Radiology, Stanford University, Stanford, CA, USA
[2] Stanford Cardiovascular Institute, Stanford University, Stanford, CA, USA
[3] Department of Medicine, Massachusetts General Hospital, Boston, MA, USA
[4] Department of Mechanical and Aerospace Engineering, University of Central Florida, Orlando, FL, USA

Abstract. Porcine hearts (N=14) underwent *ex vivo* diffusion tensor imaging (DTI) at 3T. DTI analysis showed regional differences in helix angle (HA) range. The HA range in the posterior free wall was significantly greater than that of the anterior free wall (p=0.02), the lateral free wall (p<0.001) and the septum (p=0.008). The best-fit transmural HA function also varied by region, with eight regions best described by an *arctan* function, seven by an *arcsine* function, and a single region by a *linear* function. Tractography analysis was performed, and the length that the tracts spanned within the epicardial, midwall, and endocardial segments was measured. A high number of tracts span the epicardial and mid-wall thirds, with fewer tracts spanning the mid-wall and endocardial thirds. Connectivity analysis of the number of tracts connecting different ventricular regions showed a high prevalence of oblique tracts that may be critical for long-range connectivity.

Keywords: MRI · Diffusion tensor imaging · Cardiac tractography · Connectivity · Cardiomyocyte orientation · Cardiac microstructure

1 Introduction

The structure of the heart is fundamentally connected with its function. While cardiomyocytes contract only ≈14% [8], the ventricular wall achieves ≈30-40% thickening [11]. This wall thickening is facilitated by the structural organization of the myocardium: cardiomyocytes vary in orientation through the transmural span of the ventricular wall [15] and are grouped into sheetlet structures that allow meso-scale shear [5, 17, 19]. Additionally, cardiomyocytes are both electrochemically and mechanically coupled, and transmit electrical activation and contractile forces throughout the heart. These electrochemical and mechanical couplings are supported by the continuously branching syncytium of the myocardium comprised of cardiomyocytes that have a branching structure [18].

⋆ **Co-first authors**: the first two authors contributed equally.

Diffusion tensor magnetic resonance imaging (DTI) measures the diffusion tensor of water within biological tissue. In the myocardium, the primary eigenvector (E1) of the diffusion tensor has been shown to correspond to the aggregate cardiomyocyte long axis orientation ("myofiber" orientation) within a voxel. The helix angle (HA) measures the aggregate cardiomyocyte orientation and can be measured using DTI even in live hearts [8]. Diffusion tractography connects adjacent E1 voxels into *tracts* to describe long-range connectivity [13]. While histology provides the ability to measure long-range connectivity along cut surfaces [6], three dimensional whole-heart DTI allows measurement of aggregate cardiomyocyte tracts across the whole heart [14].

Aggregate cardiomyocyte HA is fundamental to the structure-function of the heart, but there is still no consensus in terms of the best epicardial and endocardial HA values. Even within a single species (Wistar-Kyoto rat) HA range has been measured as ≈125° (epi = -50°, endo = +75°) using propagation-based X-ray phase contrast imaging [2] versus ≈180° (epi = -90°, endo = +90°) using DTI [3]. There is a lack of consensus within the literature as to the function that best represents transmural HA. Studies have shown different transmural HA functions, including *arctan* [7], *linear* [10], and *arcsine* [15] functions.

In this study we used *ex vivo* porcine cardiac DTI to examine HA range, median HA value, and the best-fit transmural HA function in different ventricular regions, utilizing a relatively large sample size. Additionally we performed diffusion tractography, and analyzed these tracts to measure the long-range connectivity between different regions of the heart.

2 Materials and Methods

2.1 Image Acquisition

This study utilized healthy swine (N=14) in accordance with institutional approvals (UCLA ARC protocol # 2015-124). Subjects underwent *in vivo* cardiac MRI using a clinical 3T scanner (Siemens, Prisma), including bSSFP 2D cine image acquisitions. After *in vivo* imaging, the subjects were euthanized and the hearts explanted. Each heart was washed with saline/water and then placed in a container filled with Fomblin. Two methods were used to support the *ex vivo* hearts in a physiological configuration: six (n=6) hearts were prepared using rapid-setting dental gel and sponges; eight (n=8) hearts were prepared using 3D printed molds based on the cine images acquired *in vivo* and segmented at mid diastole (diastasis) [1]. Within 2-3 hours from extraction, *ex vivo* cardiac DTI was performed at 3T with spatial resolution $1 \times 1 \times 1\text{mm}^3$, b-value 1000s/mm^2, 30 diffusion directions, and 5 averages. The 3D imaging volumes encompassed both the left and right ventricles. The hearts were imaged while fresh, and were not fixed.

2.2 Image Processing

Ex vivo imaging data was manually segmented by a single observer. Myocardial segmentation was performed using the DTI images, with the papillary muscles

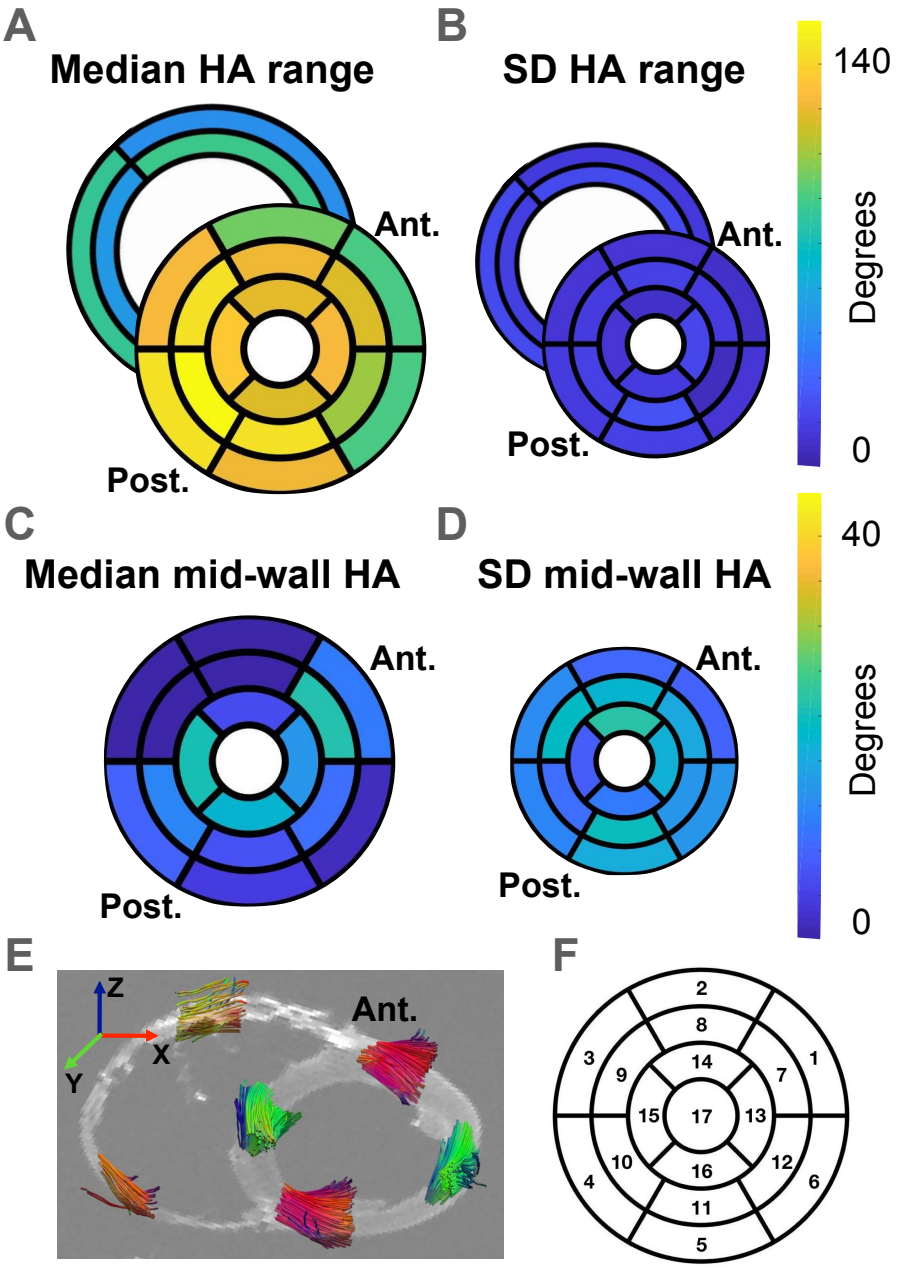

Fig. 1. Regional helix angle range and median mid-wall helix angle: Helix angle (HA) range is shown across regions of the heart (A) as well as its standard deviation (B). Also shown is the median mid-wall HA (C) and the standard deviation of mid-wall HA across all hearts (D). A 3D visualization shows the orientation of tracts within different left and right ventricular regions (E). For reference, the American Heart Association 17-segment bullseye model is also shown (F).

excluded. The cardiac long-axis was defined as the axis extending through the apex of the heart and the middle of the mitral valve. A short axis plane was defined as any plane perpendicular to this long-axis. These definitions allowed consistent prescription of short-axis planes to produce consistent HA measurements. HA was calculated as the angle between the projection of E1 onto the epicardial surface and the circumferential direction.

The LV was divided into 17 segments according to the American Heart Association (AHA) 17-segment model. The RV was divided into 4 segments: anterior base, posterior base, anterior apex, and posterior apex. For each segment of each heart, three different transmural HA functions were fit to the DTI data: (i) *linear*; (ii) *arcsine*; and (iii) *arctan*. For each region of each heart, the best-fit HA function was selected as the one with the highest coefficient of determination (R^2). Then the generalized regional best-fit HA function was determined as the mode best-fit function for that region over all of the hearts.

2.3 Tractography Analysis

Tractography was applied to E1 data using BrainSuite (Los Angeles, CA, USA) [12]. Tracts were seeded in each voxel and a step size of 1 mm was used with an angle threshold of 30^o. Tracts were terminated after 500 steps. For each tract, we quantified its longitudinal (l), circumferential (c), and radial (r) spans. We also defined the transmural trajectory (endo $r = -1$ and epi $r = 1$) of a tract as the length within the endocardial ($r \in [-1, -1/3]$), mid-wall ($r \in [-1/3, 1/3]$), and epicardial ($r \in [1/3, 1]$) transmural thirds.

Connectivity analysis was performed within BrainSuite. Tracts with length greater than 100mm were included for analysis. The connectivity (C_{AB}) between two segments (S_A, S_B) was computed as the average of two tract counts: (i) the tracts starting in S_A and ending in S_B; and (ii) the tracts starting in S_B and ending in S_A. This averaging ensured that $C_{AB} = C_{BA}$.

2.4 Statistical Analysis

The distributions of HA ranges and mid-wall HAs were non-Gaussian. We therefore used the median as the measure of central tendency. For two-group comparisons, we used a Wilcoxon signed-rank test with a least significant difference approach to correct for multiple testing. For multiple group comparisons we used a Kruskal-Wallis test.

3 Results

HA range varied across different regions of the heart (Fig. 1A). In the LV, the anterior regions tended to have a lower HA range than the posterior regions. The largest HA range was measured in the posterior free wall; this HA range was significantly larger than the HA range in the anterior free wall (p=0.02), lateral free wall (p<0.001), and the septum (p=0.008). The RV anterior free wall had

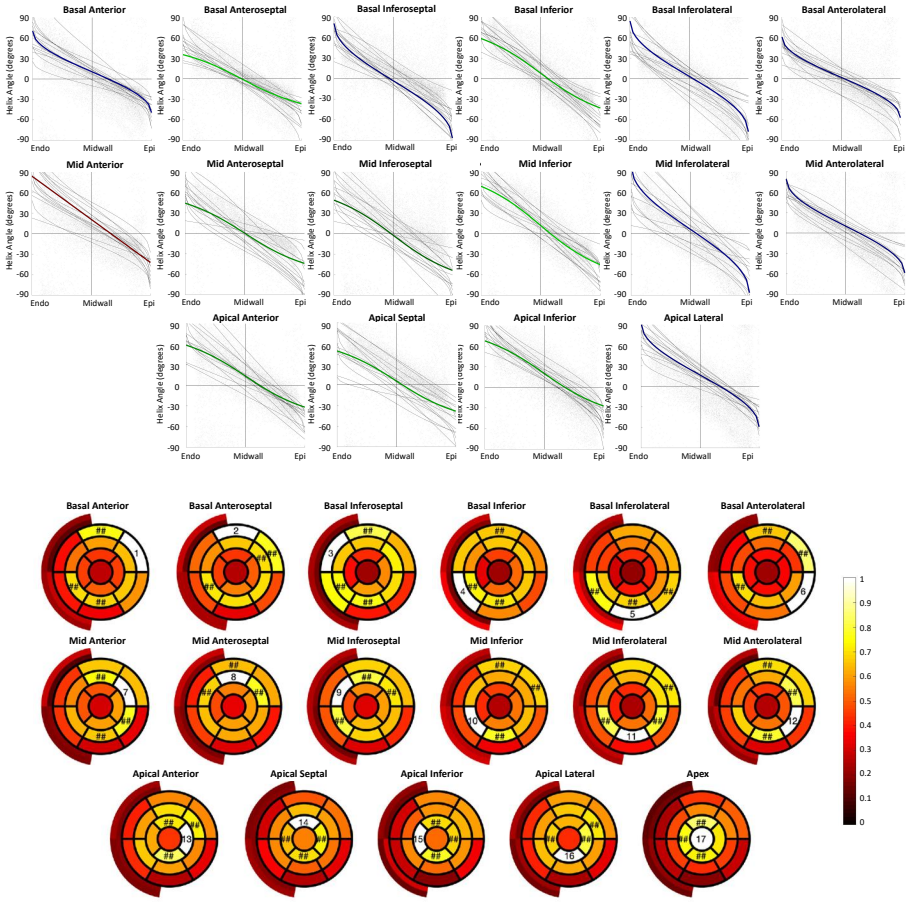

Fig. 2. Best-fit transmural helix angle function (top): For each left ventricular region, the best-fit transmural helix angle function is shown as an *arctan* function (green), an *arcsine* function (blue), or a *linear* function (red). Fits for individual hearts are shown in grey. **Connectivity analysis (bottom):** For each segment, the degree of connectivity is shown between the target region (white, numbered) and each other region. The three regions with the highest connectivity with the target region are indicated with '##'.

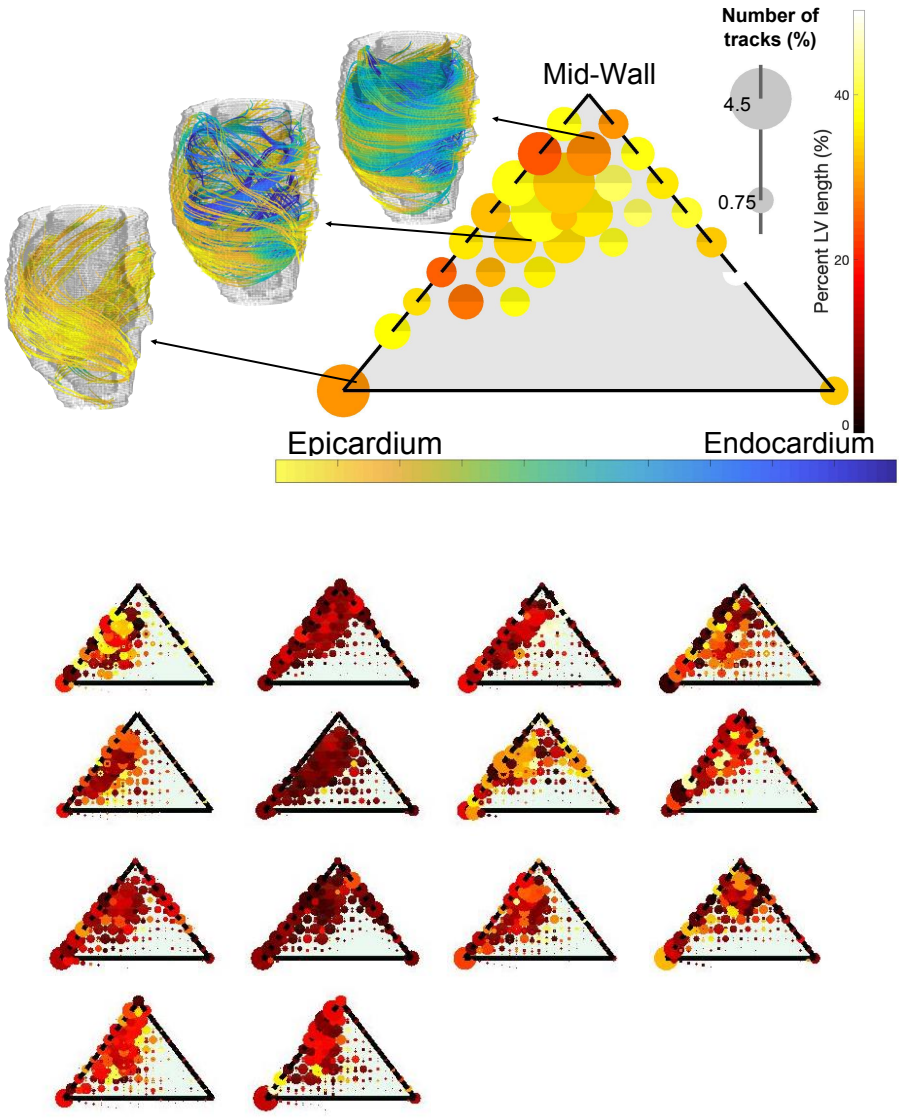

Fig. 3. Transmural analysis of the tractography data: Tracts were grouped according to their length span within each of the transmural endocardial, midwall, and epicardial thirds. Data is visualized using a barycentric coordinate system where the left, top, and right corners represent tracts spending the majority of their length in the epicardial, midwall, and endocardial thirds. An example heart is shown (top), with data on the barycentric graph corresponding with tract visualizations. The transmural spans are shown for all (N=14) hearts (bottom).

a significantly lower HA range than the RV posterior free wall (p=0.03). The standard deviation of HA range was not significantly different between segments (Fig. 1B). The median mid-wall HA was $\approx 0^o$ for half of the LV regions (Fig. 1C).

The best-fit transmural HA function (Fig. 2) showed approximately an even split between regions best represented by an *arctan* function (n=8) versus an *arcsine* function (n=7). Only the mid anterior segment was best represented by a *linear* function. The lateral regions favored an *arcsine* function, while the septal regions tended to favor an *arctan* function.

Figure 2 shows the connectivity across the 21 segments of the LV and RV. Segments typically share the greatest degree of connectivity with their adjacent segments within their short-axis plane. Unexpectedly, there is a trend of connectivity between basal anterior and posterior midwall segments, indicative of long-range oblique connections spanning at least half of the LV circumference.

Tracts were subsequently grouped according to the proportion of their length within the epicardial, mid-wall, and endocardial transmural thirds of the LV wall. A barycentric coordinate system based on the length proportions in the transmural LV segments was used to visualize these results (Fig. 3). In this reference system, tracts in the center of the triangle have equal length spans in the epicardial, mid-wall, and endocardial thirds of the LV wall. In addition to the position within the barycentric coordinate system, the circle size of the data points is proportional to the size of the tract population with given length spans. All subjects show a dense cluster on the left-hand side of the triangle, indicating a large number of tracts spanning the epicardial third and the midwall third. There is almost a complete absence of tracts that lie exclusively in the midwall (clusters at the top of the triangle). There is also a relatively low number of tracts that run only in the midwall and endocardial (right corner) thirds.

4 Discussion

In this study we present a regional comparison of transmural HA range, median, and best-fit HA function to better understand regional differences in aggregate cardiomyocyte orientation. Also, to our knowledge, this study is the first using tractography to demonstrate the long-range connectivity of ventricular segments.

Computational modeling studies of the heart require the definition of HA in all areas of the myocardium. Typically, the same HA profile is applied throughout the LV, for instance varying from -60^o at epicardium to $+70^o$ at endocardium with a *linear* transmural interpolation [4]. However, our results indicate that the transmural HA variation is likely better represented with an *arcsine* or *arctan* interpolation, as opposed to a *linear* function. Additionally, there are significant differences in HA ranges across different regions of the heart. We suggest that researchers performing computational modeling studies implement region-specific HA range and transmural HA function.

An accurate knowledge of the functional form of HA transmural variation has important consequences. Transmural HA affects the regional mechanics of cardiac contraction and therefore the ventricles' kinematics at the regional and

global levels. Furthermore, aggregate cardiomyocyte orientation is related to the fastest direction of electrical conduction in cardiac tissue and therefore HA transmural variation directly affects cardiac electrophysiology. Different studies have shown different transmural HA functions, including *arctan* [7], *linear* [10] and *arcsine* [15] functions, and there is a lack of agreement within the literature regarding which transmural HA function is most appropriate. To our knowledge this is the first study to identify regional differences in best-fit transmural helix angle function.

The high degree of connectivity between adjacent regions within the same short-axis plane was expected. However, the high number of oblique tracts connecting anterior and posterior regions at different longitudinal locations was an unexpected finding. The transmural tract data shows a predominance of tracts within the epicardium and midwall; it is likely that the tracts connecting the anterior and posterior regions have length spans primarily in these transmural regions. The high degree of connectivity would allow for increased redundancy in both electrochemical and mechanical coupling, which indicates the importance of connections between these regions. Additionally, oblique tracts may play a key role in generating ventricular torsion, and this result is consistent with cardiac structure facilitating ventricular torsion.

We propose two reasons for the low presence of endocardial tracts relative to epicardial tracts. Firstly, there is a geometric effect – the epicardial region has a greater radius – leading to a greater three dimensional volume, and therefore a greater potential to contain tracts. This factor should increase the proportion of epicardial tracts relative to endocardial tracts (circle size in Fig. 3), but not their absence from the endocardial region. Secondly, there are organizational differences between the epicardium and endocardium. Compared with the well-defined, relatively smooth epicardial surface, the endocardium contains trabeculae and papillary muscles that complicate the mesostructural organization of endocardium. This may lead to tracts that terminate at less than 100mm, which would lead to the absence of data (lack of circles in Fig. 3).

Limitations. As the hearts were imaged *ex vivo*, their MRI properties may have changed slightly as compared to *in vivo* imaging. However, we do not expect the cardiomyocyte orientations to have changed, and so this should have minimal effect on the reconstructed diffusion tensor. In terms of segmentation of the myocardium, only a single researcher performed the segmentation leading to the possibility of observer bias. However, the single observer is experienced in this type of segmentation. One limitation of DTI is that estimates of E1 have greater uncertainty within regions that are relatively isotropic. Future work could explore this limitation further. Additionally, by imaging the hearts *ex vivo* we are only able to estimate aggregate cardiomyocyte orientation in a single cardiac phase. Work from our group has shown that HA range changes through the cardiac cycle [9]. With regards to tractography analysis of cardiac diffusion tensor data, we did not perform additional validation in this study. However, it has been previously shown that tractography of *ex vivo* cardiac diffusion tensor data aligns

with tractography from high resolution synchrotron radiation imaging, and that both display the expected helix angle measurements [16].

5 Conclusion

DTI analysis of *ex vivo* porcine hearts showed regional differences of both HA range and best-fit transmural HA function. Novel connectivity analysis of diffusion tractography data revealed a high degree of long-range connectivity between oblique regions.

Acknowledgements

This material is based upon work supported, in part, by American Heart Association Grant 19IPLOI34760294 (to D.B.E.) and National Heart, Lung, and Blood Institute Grants R01-HL131823 (to D.B.E.), R01-HL152256 (to D.B.E.), and K25-HL135408 (to L.E.P.) and by the National Science Foundation under Grants 2205043 (to L.E.P.) and 2205103 (to D.B.E.).

References

1. T. E. Cork, L. E. Perotti, I. A. Verzhbinsky, M. Loecher, and D. B. Ennis. High-Resolution Ex Vivo Microstructural MRI After Restoring Ventricular Geometry via 3D Printing. In *Functional Imaging and Modeling of the Heart: 10th International Conference, FIMH 2019, Bordeaux, France, June 6–8, 2019, Proceedings 10*, volume 1, pages 177–186, 2019.
2. H. Dejea, P. Garcia-Canadilla, A. C. Cook, E. Guasch, M. Zamora, F. Crispi, M. Stampanoni, B. Bijnens, and A. Bonnin. Comprehensive Analysis of Animal Models of Cardiovascular Disease using Multiscale X-Ray Phase Contrast Tomography. *Scientific Reports*, 9(1):1–12, 2019.
3. A. Giannakidis and G. T. Gullberg. Transmural Remodeling of Cardiac Microstructure in Aged Spontaneously Hypertensive Rats by Diffusion Tensor MRI. *Frontiers in Physiology*, 11(March):1–12, 2020.
4. A. I. Hasaballa, V. Y. Wang, G. B. Sands, A. J. Wilson, A. A. Young, I. J. LeGrice, and M. P. Nash. Microstructurally motivated constitutive modeling of heart failure mechanics. *Biophysical journal*, 117(12):2273–2286, 2019.
5. I. LeGrice, Y. Takayama, and J. Covell. Transverse shear along myocardial cleavage planes provides a mechanism for normal systolic wall thickening. *Circulation research*, 77(1):182–193, 1995.
6. P. P. Lunkenheimer, K. Redmann, N. Kling, X. Jiang, K. Rothaus, C. W. Cryer, F. Wübbeling, P. Niederer, P. U. Heitz, S. Yen Ho, et al. Three-dimensional architecture of the left ventricular myocardium. *The Anatomical Record Part A: Discoveries in Molecular, Cellular, and Evolutionary Biology: An Official Publication of the American Association of Anatomists*, 288(6):565–578, 2006.
7. J. Magat, V. Ozenne, N. Cedilnik, J. Naulin, K. Haliot, M. Sermesant, S. H. Gilbert, M. Trew, M. Haissaguerre, B. Quesson, et al. 3D MRI of explanted sheep hearts with submillimeter isotropic spatial resolution: comparison between diffusion tensor and structure tensor imaging. *Magnetic Resonance Materials in Physics, Biology and Medicine*, pages 1–15, 2021.

8. K. Moulin, P. Croisille, M. Viallon, I. A. Verzhbinsky, L. E. Perotti, and D. B. Ennis. Myofiber strain in healthy humans using DENSE and cDTI. *Magnetic resonance in medicine*, 86(1):277–292, 2021.
9. K. Moulin, I. A. Verzhbinsky, N. G. Maforo, L. E. Perotti, and D. B. Ennis. Probing cardiomyocyte mobility with multi-phase cardiac diffusion tensor MRI. *PloS One*, 15(11):e0241996, 2020.
10. A. J. Pope, G. B. Sands, B. H. Smaill, and I. J. LeGrice. Three-dimensional transmural organization of perimysial collagen in the heart. *American Journal of Physiology - Heart and Circulatory Physiology*, 295:1243–1252, 2008.
11. E. A. Sallin. Fiber Orientation and Ejection Fraction in the Human Left Ventricle. *Biophysical Journal*, 9(7):954–964, 1969.
12. D. W. Shattuck and R. M. Leahy. Brainsuite: An automated cortical surface identification tool. *Medical Image Analysis*, 6:129–142, 2002.
13. D. E. Sosnovik, R. Wang, G. Dai, T. G. Reese, and V. J. Wedeen. Diffusion MR tractography of the heart. *Journal of Cardiovascular Magnetic Resonance*, 11(1):1–15, 2009.
14. D. E. Sosnovik, R. Wang, G. Dai, T. Wang, E. Aikawa, M. Novikov, A. Rosenzweig, R. J. Gilbert, and V. J. Wedeen. Diffusion spectrum MRI tractography reveals the presence of a complex network of residual myofibers in infarcted myocardium. *Circulation: Cardiovascular Imaging*, 2(3):206–212, 2009.
15. D. D. Streeter, H. M. Spotnitz, D. P. Patel, J. Ross, and E. H. Sonnenblick. Fiber Orientation in the Canine Left Ventricle during Diastole and Systole. *Circulation research*, 24(8):339–348, 1969.
16. I. Teh, D. McClymont, M.-C. Zdora, H. J. Whittington, V. Davidoiu, J. Lee, C. A. Lygate, C. Rau, I. Zanette, and J. E. Schneider. Validation of diffusion tensor MRI measurements of cardiac microstructure with structure tensor synchrotron radiation imaging. *Journal of Cardiovascular Magnetic Resonance*, 19:1–14, 2017.
17. A. Wilson, G. Sands, V. Wang, A. Hasaballa, B. Pontre, A. Young, M. Nash, and I. LeGrice. Myocardial laminar organization is retained in angiotensin-converting enzyme inhibitor treated SHRs. *Experimental Mechanics*, 61:31–40, 2021.
18. A. J. Wilson, G. B. Sands, and D. B. Ennis. Analysis of location-dependent cardiomyocyte branching. In *International Conference on Functional Imaging and Modeling of the Heart*, pages 189–199. Springer, 2021.
19. A. J. Wilson, G. B. Sands, I. J. LeGrice, A. A. Young, and D. B. Ennis. Myocardial mesostructure and mesofunction. *American Journal of Physiology-Heart and Circulatory Physiology*, 323(2):H257–H275, 2022.